Materials Science & Engineering C 131 (2021) 112475

Contents lists available at ScienceDirect

Materials Science & Engineering C

journal homepage: www.elsevier.com/locate/msec

Double-responsive hyaluronic acid-based prodrugs for efficient tumour targeting

Vincenzo Quagliariello [a,1], Arianna Gennari [b], Som Akshay Jain [a,2], Francesco Rosso [a], Rosario Vincenzo Iaffaioli [c], Alfonso Barbarisi [d], Manlio Barbarisi [e], Nicola Tirelli [b,f,*]

[a] Department of Cardio-Thoracic and Respiratory Science, University of Campania "Luigi Vanvitelli", 80138 Napoli, Italy
[b] Laboratory for Polymers and Biomaterials, Fondazione Istituto Italiano di Tecnologia, 16163 Genova, Italy
[c] Association for Multidisciplinary Studies in Oncology and Mediterranean Diet, 80138 Napoli, Italy
[d] Department of Human Sciences, Pegaso Online University, 80132 Napoli, Italy
[e] Department of Medical, Surgical, Neurological, Metabolic and Aging Sciences, University of Campania "Luigi Vanvitelli", 80138 Naples, Italy
[f] Division of Pharmacy and Optometry, School of Health Sciences, University of Manchester, Oxford Road, Manchester M13 9PT, United Kingdom

ARTICLE INFO

Keywords:
Hyaluronic acid
Responsive release
Boronates
Cancer
Targeted drug delivery
Field flow fractionation

ABSTRACT

Hyaluronic acid (HA)-based prodrugs bearing double-responsive (acid pH or oxidation) boronates of catechol-containing drugs were used to treat xenografted human prostate tumours (LNCaP) in SCID mice. The HA prodrugs accumulated significantly only in tumours (impressively, up to 40% of the injected dose after 24 h) and in liver, with negligible – actually anti-inflammatory - consequences in the latter. A quercetin-HA prodrug significantly slowed down tumour growth, in a dose-dependent fashion and with a much higher efficacy (up to 4 times) than equivalent doses of free quercetin. In short, boronated HA appears to be a very promising platform for targeted chemotherapy.

1. Introduction

Hyaluronic acid (HA) is a natural polysaccharide perhaps better known for its applications in the management of osteoarthritis or in cosmetic medicine; it is also a promising component of nanomedicines due to a combination of biocompatibility and potential targeting effects: its main receptor, CD44, is over-expressed both in a majority of solid cancers and in several inflammatory pathologies, where it also presides to a more efficient HA internalization. The mechanistic understanding of CD44/interactions is not complete yet [1,2]: besides the CD44 transcriptional and translational variability, the very role of CD44 is far from ascertained, and we have recently hypothesized it may be rather a selective internalizer than a primary HA binder [3]. However, there is ample evidence that HA (possibly with ancillary ligands such as mannose [4] or RGD peptides [5]) does allow for CD44-mediated cell targeting. [6] Here, we have used a human prostate cancer line (LNCaP) as a model. Its subcutaneous implantation in immunocompromised SCID mice is considered a pre-clinical standard [7–9], and has also been used to generate ectopic tumours in other anatomic locations, e.g. intraosseously [10]. LNCaP have been reported to be low or even zero in CD44 expression [11–14], also by our group [2] (and downregulated [12] or detectable [11,13] at the transcript level); however, and more accurately, LNCaP harbour a stem cell-like CD44(+) sub-population [15], which correlates with chemoresistance and aggressiveness [16]. Further, their CD44 expression is skewed towards variant 6-containing isoforms (CD44v6) [17], which are markers of malignancy in human prostate cancer.

As a drug, we have used a flavonoid. This class of natural polyphenols (often containing catechols, i.e. 1,2 aromatic diols) are best known for their oxidant/radical scavenging abilities [18], often considered in pathological scenarios including both cancer therapies [19,20] and in chemoprevention [21]. Quercetin (3,3′,4′,5,7-pentahydroxyflavone) is one of the most researched flavonoid [22], with a rather attractive a half-life time in plasma of about 1 day both in humans [23,24] and rodents [25], followed by a very significant elimination through the bile [26]. Its use has been hampered by a variable bioavailability, due to differences between its natural forms (various glycosides) and its synthetic, poorly soluble and more oxidizable

* Corresponding author at: Laboratory for Polymers and Biomaterials, Fondazione Istituto Italiano di Tecnologia, 16163 Genova, Italy.
E-mail address: Nicola.tirelli@iit.it (N. Tirelli).
[1] Current address: Division of Cardiology, Istituto Nazionale Tumori-IRCCS-Fondazione G. Pascale, Napoli, Italy.
[2] Current address: Sun Pharma Industries Ltd. Malanpur, Madhya Pradesh, India.

https://doi.org/10.1016/j.msec.2021.112475
Received 17 June 2021; Received in revised form 30 September 2021; Accepted 1 October 2021
Available online 12 October 2021

aglycone [27,28]. In order to improve its bioavailability, a number of nanomaterial-based formulations have been employed, including some based on HA, e.g. in chitosan/hyaluronic acid multi-layered capsules [29], or in HA-coated nanoparticles [30,31]; in some cases, quercetin has been chemically linked to HA in the form of micelle-forming macromolecular prodrugs, e.g. via NHS ester/hydrazine chemistry [32], or direct esterification [33] or through reducible disulfide-containing bridges [34]. Here we have focused on a completely soluble prodrug to eliminate any potential biodistribution variability owing to the effects of strong dilution (upon injection) on self-assembly, and on a double environmentally responsive bridge to accelerate quercetin release in a tumoural environment. The latter takes the form a boronic ester (Fig. 1A), which is stable at neutral or mildly basic pH (kd in the hundreds of micromolar), but can be cleaved upon mild acidification (pH 5–6) or exposure to stoichiometric amounts of hydrogen peroxide [35].

2. Materials and methods

2.1. Materials

Hyaluronic acid with $\overline{M_v}$ (viscosimetric average molecular weight) = 200 kDa was obtained from Fidia S.p.A (Italy). 3-aminophenylboronic acid (3-APBA) and 4-(4,6-dimethoxy-1,3,5-triazin-2-yl)-4-methylmorpholinium chloride (DMTMM), fluorescein-5-isothiocyanate (FITC), rhodamine isothiocyanate, dopamine hydrochloride, dimethyl sulfoxide (DMSO) 99.5%, ethanol 99.5% quercetin ≥95% (HPLC), piceatannol, glucose oxidase (product code: G2133) and catalase (product code: E3289) were purchased from Sigma Aldrich (Milan, Italy). All the solvents used were of HPLC grade and purchased again from Sigma Aldrich. Dialysis membranes (10 kDa MWCO) were purchased from Spectra/Por Laboratories, Inc. For cellular studies, we used human prostate cancer cells (LNCaP, ATCC® CRL-1658) that were cultured in RPMI-1640

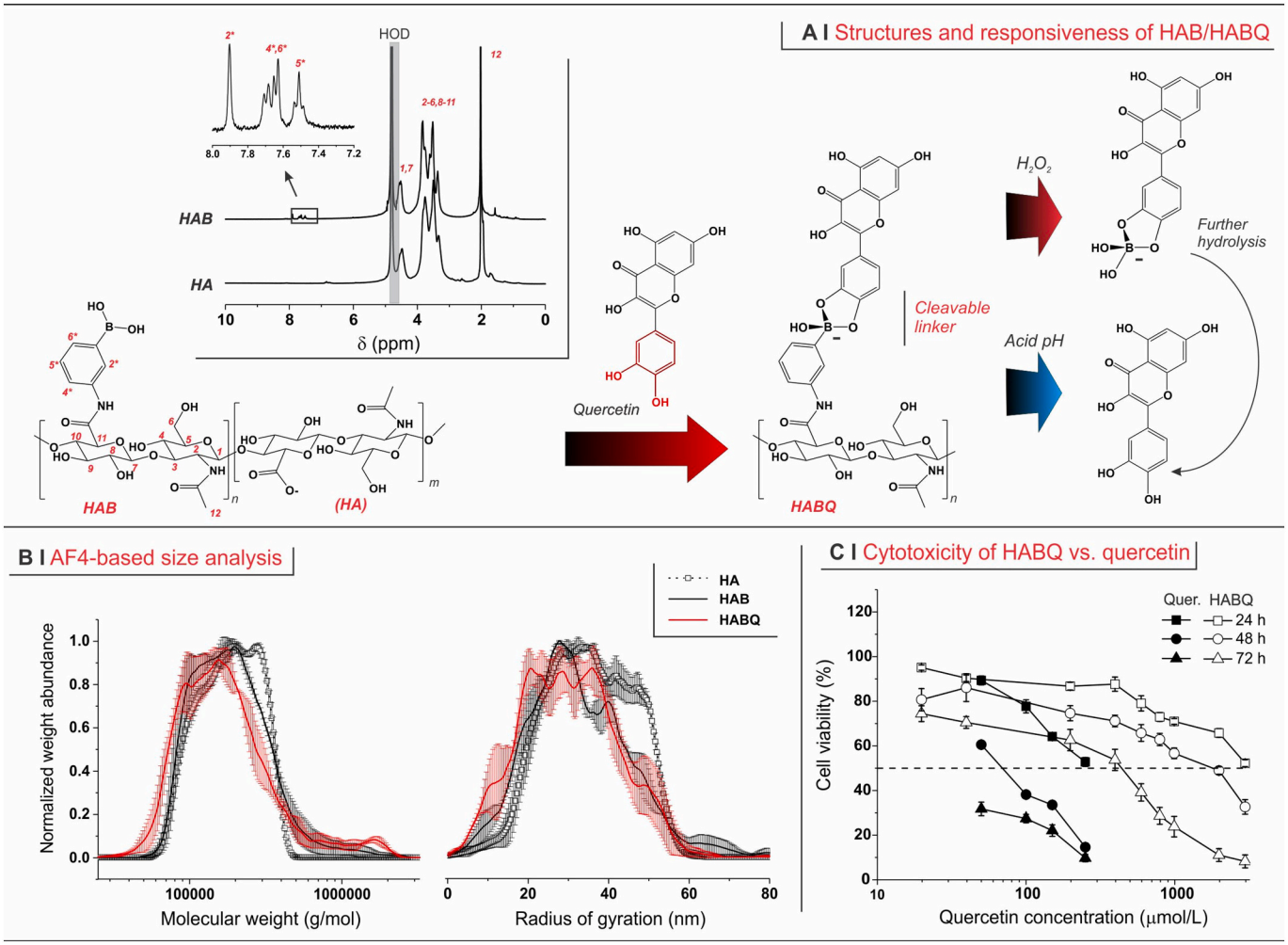

Fig. 1. *A.* HAB (*left*) boronic acids are introduced via amidation of HA carboxylic groups with 3-APBA (aromatic groups clearly visible in the ^{1}H NMR spectrum of HAB; a grey bar covers the water signal, and resonances are numbered in reference to the groups identified in the chemical structure; a star identifyies protons unique to boronate units). The ratio between functionalized and non-functionalized units, i.e. the ratio the indices *n* and *m* in the structure, is 0.316 (24:76). Boronates bind catechols and reversibly release them at low pH (transition of boronic esters from quaternarized to trigonal form followed by hydrolysis), or in the presence of oxidants such as H_2O_2 (oxidative cleavage of aromatic carbon-boron) [35]; in the latter case an boric ester is likely present as a rapidly hydrolyzing intermediate. *B.* Molecular weight (left) and radius of gyration (right) weight distribution for HA, HAB and HABQ obtained via FFF in asymmetric flow (AF4). $n = 3$. Please note that the introduction of boronic groups determines a ≈ 30% increase in molecular weight, but no significant change in the dimension of the macromolecular coil (supporting information in [35]), due to the HA chain becoming less rigid as a result of the interruption of the H bond chain between acetamide and carboxylate groups. *C.* The viability of LNCaP was assessed after 24, 48 and 72 h of exposure at 37 °C by measuring their mitochondrial reductase activity (MTT assay) as a function of the concentration of quercetin and of HABQ (both expressed as the molar concentration of the quercetin payload; please note that HABQ bears 0.396 mmol quercetin per gram). The results were normalized against the protein content of the samples, thereby provide a metabolic activity 'per cell' ($n = 3$). HABQ bears 0.396 mmol quercetin per gram of material. The LnCAP viability upon exposure to the same concentration range (0.05–7.5 mg/mL) of HA and HAB is reported in Supporting Information, Fig. 3SI. (For interpretation of the references to colour in this figure legend, the reader is referred to the web version of this article.)

medium (Gibco) instead Fetal Bovine Serum (FBS), Penicillin/Streptomycin (10,000 U/mL) and Glutamine were purchased from Invitrogen, Life Technologies. Cytotoxicity was assessed through a modified MTT [3-(4,5-dimethyldiazol-2-yl)-2,5-diphenyltetrazolium bromide] test purchased from Dojindo Molecular Technologies Inc., Rockville, MD. Concanavalin A Tetramethylrhodamine Conjugate, used for cellular imaging studies was obtained from Invitrogen, Life Technology, Milan, Italy.

2.2. Physico-chemical measurements

2.2.1. ^1H NMR

Lyophilized samples (HA and HAB) were re-dissolved in D_2O at a concentration of 1 wt%; ^1H NMR spectra were recorded using a 300 MHz Bruker spectrometer. The molar percentage of derivatization was calculated on the basis of the ratio between the integrals of aromatic resonances (related to 3-APBA and corresponding to 3 protons in each funtionalized unit) and that of the acetyl group (still 3 protons but in all units).

2.2.2. Fluorescence and UV–Vis

A Tecan Infinite M200 plate reader (I-control software) operating at 25 °C was employed for all fluorescence readings, using A) filters at 485 ± 20 nm (fluoresceinamine excitation) and 560 ± 10 nm (rhodamine emission) for FRET (Fluorescence Resonance Energy Transfer), B) filters at 485 ± 20 nm (fluoresceinamine excitation) and 528 ± 20 nm (fluoresceinamine emission) for cell uptake or biodistribution experiments. For FRET measurements, the macromolecular model compounds were dissolved at a concentration of 100 μg/mL in 10 mM acetic acid buffer at pH 3.7 and 5, in 10 mM phosphate buffer at pH 6, 7 and 7.5, or in Tris buffer at pH 8 and 8.5, and FRET measurements were conducted in 96-well black plate. The same plate reader was also employed for the fixed wavelength (450 nm or 562 nm) absorbance readings in the MTT and BCA assays used to assess cytotoxicity.

2.2.3. Static light scattering (SLS) and composition-gradient multi-angle static light scattering (CG-MALS)

Measurements were carried out using a Calypso automated delivery system as a mixing unit equipped with 0.1 μm cellulose acetate filters, connected to a Dawn Heleos II multi-angle light scattering (MALS) and a T-rEX refractive index (RI) detector, both operating at 660 nm (all instruments produced by Wyatt Technology, Santa Barbara, California). HA, HAB and HABQ were dissolved overnight in PBS (pH 7.4) at a nominal concentration of 3.0 mg/mL and then filtered twice with a 0.2 μm cellulose acetate syringe-filter. The actual concentration of HAB in the quercetin conjugate (HABQ) was calculated as follows: the sample was collected after SLS analysis, dialyzed first against 1 μM HCl and then against MilliQ water for 24 h, and the weight recovery after freeze drying was used to back-calculate accurately the initial HABQ concentration. Sample solutions were obtained in situ within the Calypso mixing unit, by diluting a stock solution with its own buffer and producing eleven concentrations ranging between 3.0 and 0.2 mg/mL. Injection volume and flow rate were fixed at 1.0 mL and 0.5 mL/min, respectively. A delay time of 60 s was set between each injection.

The Calypso software was used to collect and analyze refractive index and SLS data, assuming dn/dc = 0.13 L/g for HA and its derivatives and the actual concentration of all components to equate their nominal values using. The Zimm formalism (1st order in concentration and 1st order in angle) was selected to yield the second virial coefficient (A_2) of the samples. Representative Zimm plots are provided in Supporting Information, Fig. 1SI.

2.2.4. Asymmetric Flow Field-Flow Fractionation (AF4)

An AF2000 TM (Postnova Analytics, Landsberg, Germany) AF4 system was coupled online to PN3609 multi-angle light scattering (MALS) (Postnova Analytics, Landsberg, Germany) and PN3150 refractive index (Postnova Analytics, Landsberg, Germany) detectors in the given order. The AF4 channel was equipped with a 350 μm spacer and a 10 kDa MWCO membrane of regenerate cellulose as accumulation wall. All samples were dissolved and eluted in 10 mM phosphate/100 mM $NaNO_3$ at pH 7.4 supplemented with 0.02% (w/v) NaN_3 and filtered through a 0.1 μm filter. In a typical experiment, the detector flow rate was set at 1 mL/min and 50 μL of a 5 mg/mL solution were injected over 4 min setting 0.2 mL/min as injection flow rate. The initial cross flow was set at 2.5 mL/min. For the elution step the cross flow was maintained constant at 2.5 mL/min for 0.5 min and then exponentially (exponent = 0.30) decreased to 0 mL/min over 20 min, subsequently it was kept at 0 mL/mi for additionally 5 min. The data collected by the MALS and refractive index detectors were analysed on an AF2000 software (Postnova Analytics) and fitted with a random coil model to obtain the molecular weight and radius of gyration distribution. All samples were injected 3 times to ensure reproducibility and exclude membrane absorption. A buffer injection was also performed in order to determine the RI baseline.

2.2.5. HPLC and drug release studies

An Agilent 1200 Infinity series equipped with a C18 column (2.1 mm × 250 mm) and a UV detector, and operating at 1 mL/min and 20 °C, was employed to measure the concentration of active principles (λ = 370 nm for quercetin analysis, at 325 nm for piceatannol analysis). A literature [36] gradient elution protocol was employed, which used a mixture A composed of 19% acetonitrile, 5% methanol and 1% THF in water adjusted to pH 3 with acetic acid, and a mixture B composed of 55% acetonitrile and 15% methanol in water, always adjusted to pH; in detail, the protocol had 0–15 min, 2% B; 15–28 min, 2–28% B; 28–40 min, 28–36% B; 40–44 min, 36%B; 44–45 min, 36–80% B; 45–52 min, 80% B.

2.3. Preparative operations

2.3.1. Boronated HA derivatives

2.3.1.1. Boronated HA (HAB). 40 mg (corresponding to 106 μmol of carboxylic groups) of HA were dissolved in 10 mL of distilled water and 28 mg of 4-(4,6-dimethoxy-1,3,5-triazin-2-yl)-4-methylmorpholinium chloride (DMTMM, 100 μmol) were added to the solution. After 10 min, 1 mL of an 8.6 mg/mL solution of 3-aminophenylboronic acid (3-APBA, 63 μmol) in deionized water was added to this mixture and allowed to stir overnight at room temperature. The product was precipitated in cold ethanol and dialysed against deionized water using regenerated cellulose Spectrum Spectra/Por dialysis membranes with MWCO = 10,000 g/mol, in order to remove excess of DMTMM, its by products and any unreacted 3-APBA. Upon completion of dialysis (drop in conductivity in the dialyzed water), the solution was freeze dried. Average yield (weight of recovered material/weight of recoverable material) = 75–85%wt. A degree of derivatization of 24%mol (of carboxylic acids) was obtained through ^1H NMR spectra, by using the integral of 3-APBA aromatic resonances and that of the HA *N*-acetyl methyl group (dividing the first by 4 and the second by 3, their ratio provides the ratio between the numbers of functionalized and total repeating units). This corresponds to 0.60 mmol of boronates per gram of material.

^1H NMR (D_2O): δ = 7.76–7.81 (H2*), 7.49–7.6 (H4*, H6*), 7.36–7.42 (H5*), 4.3–4.5 (H1, H7), 3.1–3.8 (H2 to H6 and H8 to H11), 1.8–1.9 ppm (H12). For proton numbering refer to Fig. 1A.

2.3.1.2. Fluorescein-labelled HAB (FA-HAB). 50 mg of HAB (corresponding to 97 μmol of carboxylic groups) were dissolved in 40 mL of distilled water and diluted with 20 mL of DMSO. A solution of 25 mg (75 μmol) of fluoresceinamine, 25 μL of acetaldehyde (440 μmol) and 25 μL of cyclohexyl isocyanide (250 μmol) in 100 μL of DMSO was added to the HAB solution. After stirring overnight, the polymer was precipitated

three times in cold ethanol, until complete disappearance of fluorescein fluorescence in ethanol, and freeze dried. Yield: 80–85% in weight. Using a calibration with free fluoresceinamine, the degree of fluorescein labelling was determined to be 0.29% mol of the total carboxylic groups.

2.3.1.3. Rhodamine-bearing FA-HAB (FRET acceptor). Dopamine hydrochloride (7.6 mg/40 μmol) was dissolved in 2 mL of thoroughly degassed methanol (to avoid catechol oxidation), together with a 2-fold molar excess of triethylamine (12 μL/86 μmol), stirring the solution for 30 min under argon. Rhodamine isothiocyanate (21 mg/40 μmol) was then added to the solution and the mixture was left under stirring at room temperature for 4 h.

20 mg of FA-HAB (corresponding to 12 μmol of boronate groups) were dissolved in 25 mL of degassed 10 mM phosphate buffer at pH 8; the previously prepared FRET acceptor solution (corresponding to 40 μmol of catechols) was diluted with 8 mL of the same PBS buffer, and the resulting mixture was added dropwise to the FA-HAB solution over 30 min. The product was then purified by dialysis against deionized water (regenerated cellulose Spectrum Spectra/Por Dialysis membranes with MWCO = 10,000 g/mol) while bubbling argon for seven days until no rhodamine fluorescence was recorded in the dialysis medium; the solution was finally freeze dried to yield 15 mg of product.

2.3.2. HAB macromolecular prodrugs

2.3.2.1. Quercetin-HAB adduct (HABQ). 5 mL of a 4 mg/mL solution of HAB (total of 12 μmol of boronate groups) in 100 mM phosphate buffer at pH 8 were mixed with 5 mL of a 2.1 mg/mL quercetin solution in the same buffer containing 10%v/v of DMSO (35 μmol of quercetin, corresponding to a ≈ 3:1 quercetin/boronate molar ratio). The solution was stirred for 30 min and then precipitated in cold ethanol, to remove unreacted quercetin. After centrifugation and evaporation of residual ethanol, the product was dissolved in 5 mL of deionized water and freeze dried. The amount of bound drug was measured by detaching quercetin (1 mg of polymer was dissolved in 1 mL of 10 mM acetate buffer at pH 4), and measuring its amount via HPLC. Quercetin content: 0.396 mmol quercetin per gram of material (70% mol functionalization of boronic acid residues). The fluorescently labelled macromolecular prodrug (**FA-HABQ**) was prepared identically, by replacing HAB with FA-HAB.

2.3.2.2. Piceatannol-HAB adduct (HABP). The protocol was identical to that used for the preparation of HABQ, only using 5 mL of a 1.7 mg/mL piceatannol solution (35 μmol of piceatannol, corresponding to a ≈ 3:1 piceatannol/boronate molar ratio). Piceatannol content: 0.438 mmol piceatannol per gram of material (77% functionalization of boronic acid residues). The fluorescently labelled macromolecular prodrug (**FA-HABP**) was prepared identically, replacing HAB with FA-HAB.

2.4. Release studies

2.4.1. Quercetin release

500 μL of a 5 mg/mL solution of HAB dissolved in water (equivalent to 1.5 μmol of boronates), 10 μL of a solution quercetin 36 mg/mL in DMSO (equivalent to 1.2 μmol) and 100 μL of a 1 M glucose stock solution in water, were mixed in a 2 mL glass vial equipped with a magnetic stirring bar. The stability of the resulting HABQ was then assessed using glucose oxidase to acidify pH, produce H_2O_2 or both, as described in the points below. In all experiments 50 μL aliquots were pipetted out at different time points and added to Eppendorf tubes containing 1 mL of ethanol each in order to precipitate all HA-containing species (HAB containing variable amounts of quercetin) and dissolve the released quercetin. All the collected aliquots were then centrifuged (16,000 *g* for 90 min), and the pellets re-dissolved in 100 mM acetate at pH 4, precipitated again in 1 mL of ethanol, centrifuged and the supernatant was finally analysed by RP-HPLC to measure the quantity of quercetin (initially still bound to HAB and then detached through acid treatment).

1) pH-induced release: water and 1 μM NaOH were added to adjust the pH to 8 and the final volume to 980 μL. The mixture was then stirred on a magnetic stirrer set at 37 °C for 5 min to allow the formation of the HABQ complex and equilibrate the temperature. Afterwards, 10 μL of a 20 mg/mL (5000 U/mL according to the manufacturer) glucose oxidase solution (product code: G2133, Sigma, Milan, Italy) and 10 μL of a 25 mg/mL (50,000 U/mL according to the manufacturer) catalase solution (product code: E3289, Sigma, Milan, Italy) were pipetted into the vial. The solution was kept under stirring at 37 °C while the pH value was continuously monitored using a microelectrode (InLab Ultra-Micro-ISM, Mettler Toledo, Milan, Italy).

2) pH- and H_2O_2-induced release: the experiment was performed as described above replacing the 10 μL of catalase with 10 μL of water. For each time point the H_2O_2 concentration was back-calculated from a master curve obtained by following the kinetic of glucose conversion in a 96 well plate. Briefly, 10 μL of 20 mg/mL glucose oxidase stock solution, 39 μL of 1 M glucose and 51 μL of substrate solution (i.e. TMB reagent) from Elisa kit CEB459Ge (Cloud-Clone Corp., DBS Italia s.r.l., Segrate, Italy) were placed in a well of a 96-well plate and equilibrated at 37 °C for 5 min inside a BioTek Synergy H1 multi-mode microplate reader (BioTek Instruments, Inc., Winooski, VT, USA). 380 μL of a 50 mg/mL (corresponding to 10,000 U/mL according to the manufacturer) solution in 100 mM phosphate buffer at pH 8 of peroxidase from horseradish (product code: P8250, Sigma, Milan, Italy) were then added and the change in absorbance at 650 nm was monitored over 1 h.

3) H_2O_2-induced release: the initial suspension was diluted with 380 μL of 100 mM phosphate buffer at pH 8 and was then stirred at 37 °C for 5 min. pH and H_2O_2 concentration were monitored as described above. Afterwards, 10 μL of a 20 mg/mL glucose oxidase (5000 U/mL) were added and the solution was kept under stirring at 37 °C.

4) Glucose-induced release: 500 μL of a 5 mg/mL solution of HAB (1.5 μmol of boronates) in water, 10 μL of a 36 mg/mL quercetin solution in DMSO (1.2 μmol) and 100 μL of either a 1 M or a 0.1 M glucose stock solution in water were mixed with 390 μL of 100 mM phosphate buffer at pH 8, or 490 μL of the buffer with no glucose. After 14 min, a 50 μL aliquot was collected as described above (see Supporting Information, Fig. 2SIA, centre and right; the control with no glucose is also presented in Fig. 2B).

2.4.2. Controls

A) Quercetin stability under oxidizing conditions. These control experiments were conducted as described above but in the absence of HA derivatives and without centrifugation (the solution was directly analysed via RP-HPLC, see Supporting Information, Fig. 2SIB). B) Quercetin retention by HA. HAB was replaced by HA, with no enzyme and 100 mM glucose, in order to assess the possible retention of quercetin by HA in the absence of covalent bonds. An aliquot was sampled after 14 min incubation at pH 8 (see Supporting Information, Fig. 2SIA, left).

2.5. Biological evaluation

2.5.1. General cell culture

Human prostate cancer cells (LNCaP, ATCC® CRL-1658) were cultured in RPMI-1640 medium (Gibco) containing 10% FBS, 1% Pen-Strep and 2 mM L-Glutamine at 37 °C in a humidified 5% CO_2 atmosphere.

2.5.2. Cytotoxicity

Cytotoxicity was assessed by evaluating the mitochondrial dehydrogenase activity through a modified MTT [3-(4,5-dimethyldiazol-2-yl)-2,5-diphenyltetrazolium bromide] test, which was implemented according to the manufacturer's instructions (Dojindo Molecular Technologies Inc., Rockville, MD). LNCaP cells were seeded in 96-well plates at a density of 10,000 cells per well under the conditions mentioned above, and the modified MTT assay was performed at 24, 48 or 72 h as a

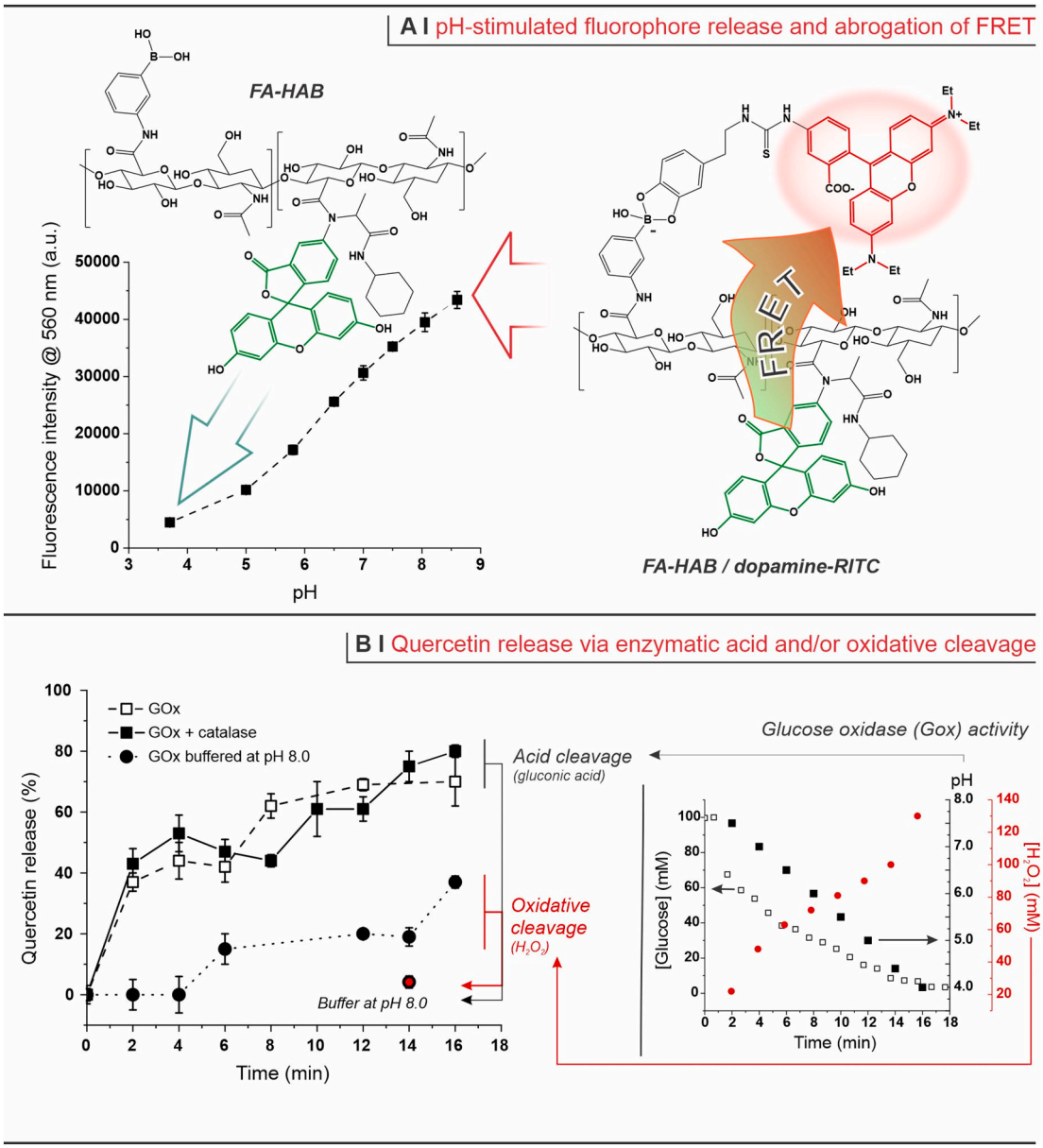

Fig. 2. *A.* Dependency of FRET efficiency (λ_{exc} = 480 nm, fluoresceinamine; λ_{em} = 560 nm, rhodamine) on pH for FA-HAB/rhodamine-dopamine (FRET acceptor). At low pH, the negligible FRET implies that the FRET acceptor (in red) has detached from the structure containing fluoresceinamine (in green). n = 3. *B.* Relative amount of released quercetin upon exposure of an initially pH = 8 solution HABQ (0.25 mg/mL corresponding 1.2 mM quercetin) to 0.2 mg/mL (50 U/mL) GOx and 100 mM glucose (white squares); in control experiments, H_2O_2 was decomposed using 0.25 mg/mL (500 U/mL) catalase (black squares), or pH was maintained at 8 by using a strong buffer, i.e. 100 mM PBS (black circles). In the presence of glucose but without GOx, the release of quercetin is negligible (about 5% after 14 min; red symbol). Please note that under these conditions and within this time frame, quercetin is not oxidized (see Supporting Information, Fig. 2SI, panel A). In the smaller graph, the increasing concentration of H_2O_2 (red circles) and decreasing pH (black squares) as a function of time. n = 3. (For interpretation of the references to colour in this figure legend, the reader is referred to the web version of this article.)

function of the macromolecular prodrug concentration. At the end of each incubation period the cells were washed three times with PBS at pH 7.4 and incubated with 100 μL of a MTT solution (0.5 mg/mL in cell culture medium) for 4 h at 37 °C. The relative cell viability (%) was calculated by the formula $[A]_{test}$ / $[A]_{control}$ × 100, where "$[A]_{test}$" is the 450 nm absorbance of the test sample, and "$[A]_{control}$" is the 450 nm absorbance of the control cells incubated solely with culture medium. The relative cell viability was then normalized against the total protein content, which was used as a measure of the cell number and was measured through the Micro BCA protein assay kit (Pierce). Briefly, the cells were washed with ice-cold PBS, and incubated for 15 min in 150 μL cell lysis buffer (0.5% v/v Triton X-100 in PBS), to which 150 μL of Micro BCA protein assay kit reagent (prepared following the instructions of the manufacturer) were added. The absorbance at 562 nm was finally measured on a plate reader. The MTS readings were then normalized by the amount of total protein content in each well. Please note that even at the HABQ highest concentration (7.5 mg/mL), the pH was not sufficiently acid to induce significant quercetin release (pH = 7.8 after 24 and 48 h, and 7.5 after 72 h; in this pH region the catechol-boronate complex is stable [35]).

2.5.3. Cell uptake

2.5.3.1. Quantification. LNCaP cells were seeded at a density of 5 × 10^3 cells/well in a 24-well plate under the conditions mentioned above and allowed to grow for 24 h. The medium was then replaced with 0.1 mL of

a 0.3 mg/mL solution of FA-HABQ in culture medium and allowed to incubate for a time comprised between 0.5 and 24 h. The experiments were terminated by removing the supernatant, washing the cells three times with 10 mM PBS and lysing the cells with 0.1 mL of 0.5% Triton X-100 in 0.2 N NaOH. The total uptake of macromolecular prodrug through the 530 nm the fluorescence of the cell lysate, employing a calibration with 0.001–0.6 mg/mL FA-HABQ dispersed in a cell lysate solution (10^6 untreated cells dissolved in 1 mL of the Triton X-100/0.2 N NaOH solution). **Imaging**. 5×10^3 cells/well were seeded in a 24-well plate under the conditions mentioned above and allowed to grow for 24 h. The medium was then replaced with anti-human CD44v6 antibody IgG1 (clone VFF7, Abcam, stock concentration 1 mg/mL) diluted 1/200 for 1 h. The wells were then washed two times with PBS, and the medium was finally replaced with a 0.3 mg/mL FA-HABQ solution in culture medium and incubated for 2 h. Subsequently, cells were thoroughly rinsed three times with PBS and fixed with a 2.5% glutaraldehyde in PBS for 20 min. Membrane staining was obtained by using Concanavalin A Tetramethylrhodamine Conjugate (Invitrogen, Life Technology) at a final concentration of 100 μg/mL. After washing in PBS, cells were blocked with 1% BSA in PBS for 20 min and washed three times with PBS. Using a Confocal Microscope (C1 Nikon) equipped with a EZ-C1 Software for data acquisition and 60× oil immersion objective, the macromolecular prodrug was imaged through excitation/emission at 492/518 nm for, and the cell membrane with excitation/emission at 555/580 nm.

2.6. In vivo studies

One hundred and ten immunodeficient mice, BALB/c Nude (seven weeks old, 20–25 g) were purchased from Charles River Laboratories, Calco, Italy. Mice were housed 6 per cage and maintained on a 12 h light-12 h dark cycle (lights on at 7.00 am) in a temperature-controlled room (22 ± 2 °C) and with food and water ad libitum. The experimental protocols were in accordance with EU Directive 2010/63/EU for animal experiments, and institutional guidelines of the Italian Ministry of Health, Animal Care and Use Committee. All animal experiments were approved by the local ethics committee, the *Organismo preposto al benessere degli animali* (OPBA). After 1 week of growth, mice were randomized and treated for biodistribution and anticancer studies as described in Sections 2.6.1 and 2.6.2.

2.6.1. Biodistribution in tumour-bearing mice

Tumour-bearing mice were prepared by injecting a suspension of LNCaP cells 1×10^6 in 100 μL of saline physiological solution into the subcutaneous space of athymic nude mice dorsa (seven weeks old, 20–25 g). After 14 days of appropriate tumour growth, FA-HABQ (0.396 mmol of quercetin per gram of material, 1:0.7 boronic acid/quercetin molar ratio), FA-HABP (0.438 mmol of piceatannol per gram of material, 1:0.8 boronic acid/piceatannol molar ratio) and FA-HAB were injected into the tail vein of the tumour-bearing mice ($n = 10$/group) at a dose of 10 mg of material per kg of weight, which corresponds to 3.96 μmol of quercetin or 4.38 μmol of piceatannol per kg of weight. After 24 h the animals were sacrificed, and tumour, spleen, heart, liver, lungs, kidneys were removed, weighed, lysed with a 5% *w/v* sodium dodecyl sulfate (SDS) solution in deionized water for 1 h prior to recording the fluoresceinamine fluorescence intensity. The values were normalized against an appropriate calibration with FA-HA derivatives in lysed organs (concentrations between 0.05 and 5 mg/mL) and expressed as μg of fluorescent macromolecular prodrug/g of tissue and percentage of injected dose per organ (% ID/organ) (see Supporting Information, Fig. 4SI).

2.6.2. Therapeutic efficacy

Tumour-bearing mice were prepared as described in Section 5.5.1SI and were divided into eight groups ($n = 10$ for each group). Treatment was initiated when the tumour volume reached 90 mm^3. The mice were then i.v. injected (tail vein) with 200 μL of the following solutions: HABQ (of 0.396 mmol of quercetin per gram of material; 1:0.7 boronic acid/quercetin molar ratio) in PBS to obtain doses of 25 and 50 mg/kg of HABQ, which correspond to 3 and 6 mg/kg of quercetin, respectively, free quercetin in PBS containing 11% wt. DMSO to obtain doses of 3, 6, 25 mg/Kg, HAB in PBS to obtain a dose of 50 mg/Kg, and DMSO 11% wt. in PBS. The tail vein injections were performed every 3 days for a total period of 21 days of treatment, following which the animals sacrificed according to ethical laws in force, following a literature method1. The tumour size was determined by caliper measurement of the largest and perpendicular diameters during the time of treatment. Tumour volumes were calculated according to the formula: $V = a * b^2 * 0.52$, where a is the largest superficial diameter and b is the smallest superficial diameter, according to a literature procedure [37].

2.7. Statistical analysis

Data are presented as means ± standard error (SE). Analysis of variance (one-way ANOVA) was performed and values of $p < 0.05$ were considered statistically significant.

3. Results and discussion

A boronated derivative (HAB) was prepared using the DMTMM-mediated amidation of HA carboxylic acids with 3-aminophenylboronic acid (3-APBA, Fig. 1A) [35], functionalizing one in four disaccharidic repeating unit (24% of carboxylic acids converted). Following a protocol previously used by our group [5] and initially developed by Crescenzi [38], HA derivatives were also labelled with fluoresceinamine through a multi-component Passerini-Ugi reaction (structure in Fig. 2A). Of note, while increasing in molecular weight, the macromolecule does not increase in size or even slightly contracts (Table 1; compare also the HA and HAB lines in Fig. 1B, right); this is a consequence of HAB's less rigid chain (derivatization interrupts the chain of intramolecular hydrogen bonds between carboxylates and acetamides in neighbouring units), although intramolecular binding of boronates to sugar diols may also play a role.

HAB was then linked to quercetin to yield a structure (HABQ) where about 1/3 of unreacted boronates, which shift the complexation equilibrium to the right and therefore allow for a high avidity and stable quercetin entrapment even if the binding constant of boronates for catechols is not extremely high (kd typically in 0.1–1 mM range). Of note, the SLS analysis of HABQ showed a negative second virial coefficient (A2) in PBS (Table 1), which indicates it considerably less hydrophilic than HAB, on its turn already less hydrophilic than its parent HA. During AF4 analysis, HABQ undergoes very high dilution (in excess of

Table 1
Physico-chemical characterization.

	$\overline{M_w}$ (kDa)[a]	Đ[a]	Rg (nm)[a,b]	A2 (mmol·mL/g^2)[b]
HA	197 ± 6	1.20 ± 0.01	34 ± 1/39 ± 1	2.99 ± 0.02
HAB	237 ± 49	1.36 ± 0.15	30 ± 2/40 ± 1	0.49 ± 0.01
HABQ	234 ± 8[c]	2.18 ± 0.83 [c]	23 ± 2[c]/34 ± 1	−0.26 ± 0.02

[a] From asymmetric flow field-flow fractionation (AF4) in 10 mM phosphate supplemented with 100 mM $NaNO_3$ (pH 7.4), using static light scattering (SLS) and refractive index detectors; the molecular weight and radius of gyration (Rg) distribution are provided in Fig. 1B. $n = 3$.

[b] The weight average value of Rg and the second virial coefficient (A2) were measured via batch SLS in 10 mM PBS (pH 7.4); the Zimm plots are provided in Supporting Information, Fig. 1SI. $n = 3$. The Rg values obtained with batch SLS and those from AF4 (with SLS detector) are slightly different, due to the different ionic composition of the solution, which causes a different coil expansion.

[c] AF4 analysis implies an in situ very high dilution (≫1:1000) and non-equilibrium (ultrafiltration-like) flow conditions, which eventually detach quercetin from HABQ. These results therefore refer effectively to a re-generated HAB.

1:10,000, much higher than e.g. upon injection in murine blood stream) under non-equilibrium conditions and quercetin is largely released, due to the well-known dynamic character of the linkage [39,40]; this allows to show that HAB survived the functionalization with essentially unaltered molecular weight and Rg distributions (Fig. 1B).

Using LnCAP as a model, HA and HAB have a negligible toxicity (see Supporting Information, Fig. 3SI, panels A and B), as it should be expected by structures chosen as carriers. The average cell viability was unaffected by HA, with incubation times up to 3 days and concentrations up 7.5 mg/mL, and only marginally decreased by HAB (no effect at 24 h, max decrease at 72 h with viability down to 70–80%). Conversely, HABQ showed a measurable and markedly time-dependent toxicity (Fig. 1C; IC50 = 7.5 mg/mL at 24 h, 5 mg/mL at 48 h and 1–1.5 mg/mL at 72 h), which at any time point, however, was about one order of magnitude lower than that of free quercetin. The lower toxicity of HABQ indicates that, under the conditions used for this in vitro test (pH buffered at neutrality; likely low LNCaP activation causing low ROS production), its boronic esters are likely to retain quercetin, at least when the construct remains in the extracellular environment. On the contrary, the observed toxicity may stem from intracellular release, since endosomal acidification would cleave quercetin from HA. Therefore, while this result is not indicative of HABQ's toxicity in the rather acidic and ROS-rich environment of a solid tumour, it ensures its rather benign character at non-tumoural sites.

The pH-dependent hydrolysis of HABQ's boronic ester was first confirmed by FRET experiments (Fig. 2A). A fluoresceinamine-labelled HAB (FA-HAB) was reacted with a rhodamine-labelled catechol (produced by reacting dopamine with rhodamine isothiocyanate), yielding an HA bearing two FRET partners. When the two fluorophores are in reasonable proximity, excitation of fluoresceinamine transfers to rhodamine: irradiation at 480 nm (fluoresceinamine) at neutral/basic pH induces a strong rhodamine emission at 560 nm. This effect weakened upon acidification, which indicates an increasing distance compatible with the cleavage of the boronic ester.

A more complete proof of double responsiveness was obtained by using glucose oxidase (GOx): GOx oxidizes glucose to gluconolactone, which rapidly hydrolyzes to gluconic acid, and produces hydrogen peroxide a byproduct (Fig. 2B). This allows quercetin release through both a stoichiometric and a catalytic mechanism, respectively the oxidative cleavage of the phenylboronic unit (and later hydrolysis of the boric ester, see Fig. 1A, right), and the acid hydrolysis of the boronate. Quercetin was rapidly reduced from HABQ during acidification, irrespective of the presence of H_2O_2 (±catalase), while the purely oxidative mechanism (with a stronger buffer) was considerably slower. Therefore, it could be hypothesized that quercetin may be released predominantly through hydrolysis in an acidic environment (tumour interstitial space, acidifying endosomes), and through oxidative cleavage when ROS are encountered under neutral conditions.

The uptake of fluorescently labelled HA derivatives was assessed by quantifying their presence in cell lysates, which reflects cell surface-bound and internalized material. HA levels in cell lysates (either soluble or in nanoparticles - at least in macrophages they have a comparable total uptake kinetics [1]) typically plateau in a few hours, probably due to saturation of receptors used in HA binding and above all in its internalization. For example, CD44 accompanies HA in its degradation in lysosomal compartments instead of being recycled to the cell surface [41–43], and indeed the plateau in HA uptake corresponds to a CD44 temporary disappearance from the cell surface [5]. The uptake of FA-HABQ followed the same trend, reaching a plateau after approximately 8 h (Fig. 3A); its fluorescence would seem associated to peripheral compartments at early time points (0.5–4 h) and to more central (possibly lysosomal) ones after 24 h. Importantly, and confirming earlier reports about the importance of CD44v6 in both invasiveness and HA interactions of LNCaP, pre-incubation with an anti-CD44v6 antibody completely blocked its uptake (Fig. 3B).

Having therefore established that HABQ preserved a receptor-mediated mechanism of internalization in the target cells, we proceeded to use a model of dorsally implanted LNCaP in SCID mice in order to assess HABQ's capacity to preferentially accumulate in their tumoural mass. The parent HAB showed very little presence in the main organs outside tumour and liver; in the latter organ, HAB dose was about twice as large as in the tumour (Fig. 4A, left). Capture in the liver is indeed almost unavoidable for HA and its derivatives, since there most HA catabolism takes place [44,45]; however, this is possibly the least potentially dangerous site of accumulation, due to liver's own regenerative capacities. This high dose in the liver may be interpreted as a form of the highly heterogenous Enhanced Permeation and Retention (EPR) effect, which is typically invoked when colloids larger than the renal filtration limit accumulate in tumours. HAB(Q) is most certainly above that limit (see Fig. 1B), but any further speculation on its dimensions is probably not meaningful: the coil size of a soluble macromolecule would markedly depend on the local osmotic (oncotic) pressure, which in a

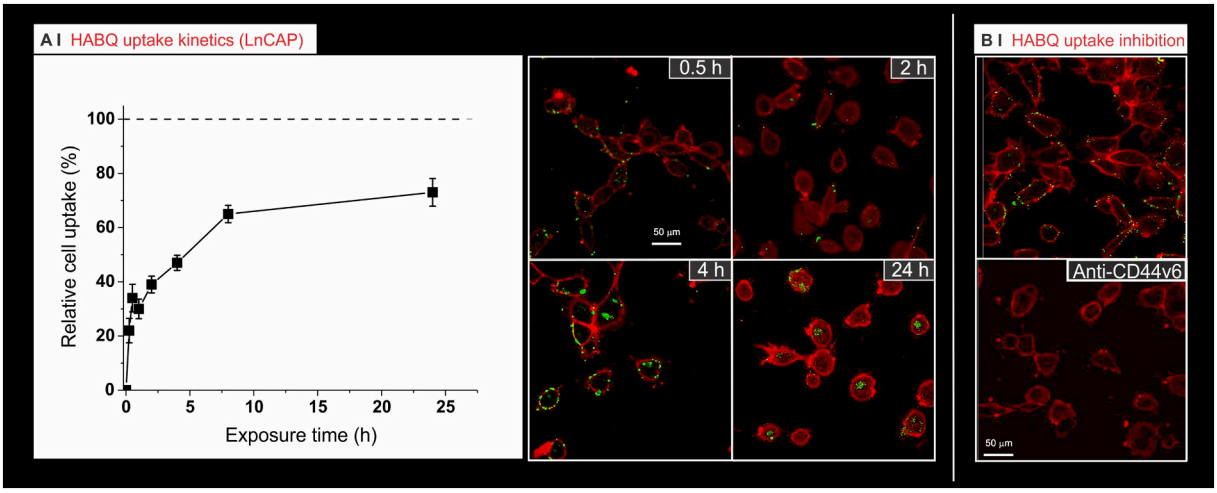

Fig. 3. *A. Left:* uptake kinetics of FA-HABQ in LNCaP (fluorescence of cell lysates) as a function of time. The 100% line corresponds to fluorescence emission of a 0.3 mg/mL solution of FA-HABQ. *Right:* Confocal images of LNCaP incubated with 0.3 mg/mL FA-HABQ (red: actin); the punctuated green fluorescence seems to indicate that HA progressively moves from a peripheral to a perinuclear localization. $n = 3$. *B.* Confocal images of LNCaP (2 h) with FA-HABQ without (above) and with (below) pre-treatment with anti-human CD44v6 antibody. (For interpretation of the references to colour in this figure legend, the reader is referred to the web version of this article.)

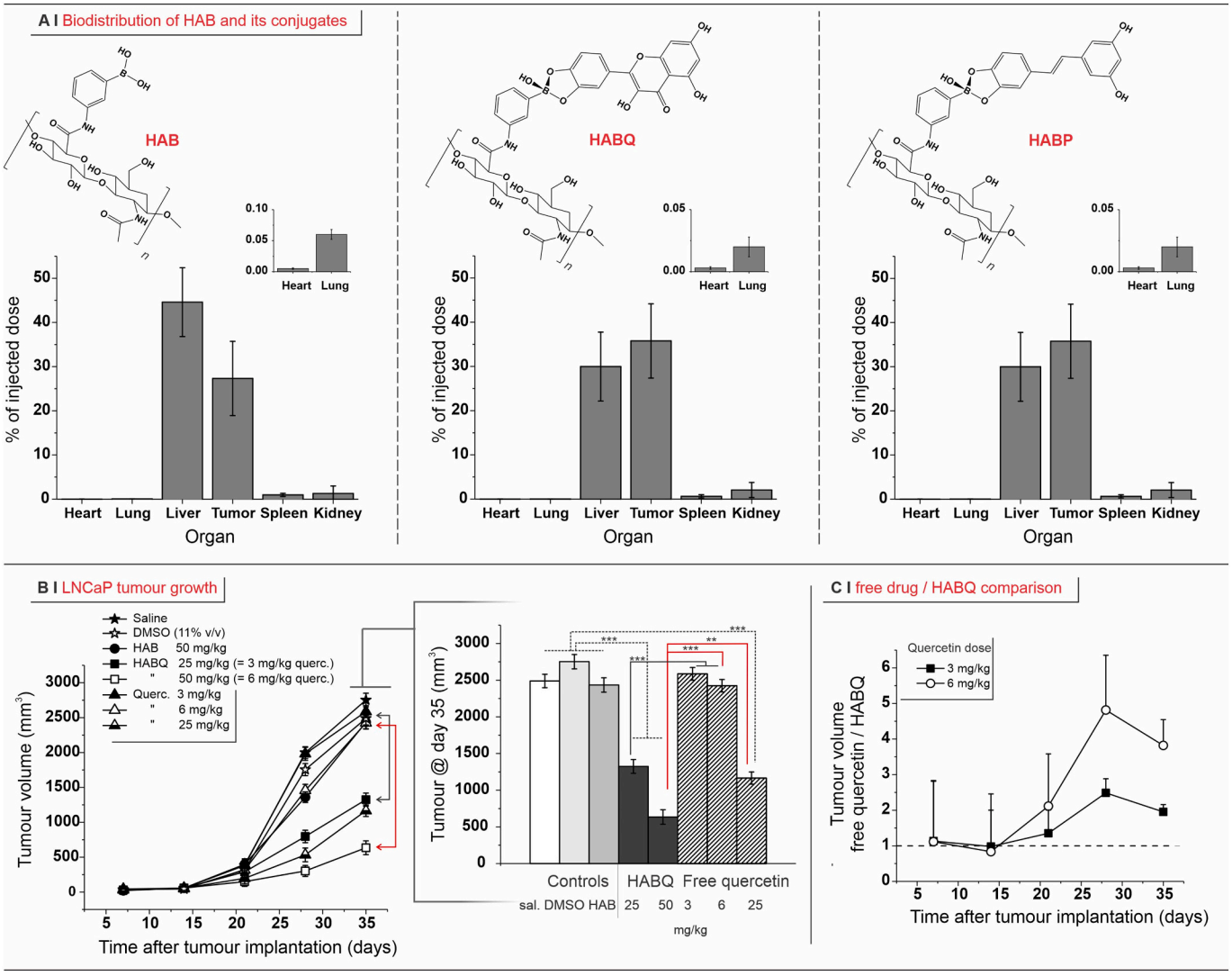

Fig. 4. *A.* wt% of the injected dose ($n = 8$) for fluorescently labelled HA derivatives (FA-HABx) in the main organs of prostate cancer-bearing SCID mice 24 h after injection in the tail vein (200 μL, 10 mg/kg); the amounts of HA derivatives are estimated on the basis of the fluorescence intensity in organ lysates. Please note that in the graphs in the left one can conclude that either about 30% of the dose is still circulating 24 h after administration, or it has been already degraded and the fluorophore excreted. Statistically, the % of injected dose in liver and tumour is never significantly different ($p = 0.3–0.7$ in one-way ANOVA comparison); however, the concentration of the HAB is statistically higher in the liver, that of HABP higher in the tumour (see Supporting Information, Fig. 4SI). *B.* Tumour volume as a function of time upon tail vein injection of quercetin formulations (free drug – triangles; HABQ – squares) and negative controls. The arrows are a guide for an easier comparison of the day 35 performance of free quercetin and HABQ with identical quercetin dosage. The inset provides the results for a one-way ANOVA comparison of the day 35 data (** $p \leq 0.01$; *** $p \leq 0.001$), showing the large, statistically relevant differences between negative controls and HABQ treatments (while this is true only for highest quercetin dose), and between HABQ formulations and free quercetin with the same or higher drug doses. $n = 8$ per time point and per formulation. *C.* The tumour volumes recorded with free quercetin are divided by those obtained with HABQ at the same quercetin dosage; this ratio quantitatively shows how more effective the prodrugs are. The largest differences are recorded at day 28 and 35 after implantation, i.e. respectively 1 and 2 weeks after the end of the treatments.

tumoural vasculature is largely unknown. Whatever the precise EPR mechanism in this case, a local enrichment due to the enhanced interactions of these constructs with CD44 on an inflamed vascular endothelium (well reported e.g. in [46,47]) may be involved.

Similarly to HAB, also HABQ showed significant accumulation only in liver and tumour, but with a higher dose in the xenograft (Fig. 4A, centre); slightly less than 40% of the injected dose was indeed found in the LnCAP tumour after 24 h, which is a very positive indication in view of a targeted therapy. HAB derivatized piceatannol (HABP) - another naturally occurring catechol, the main metabolite of resveratrol [48] – showed a similar enhanced tumour accumulation, indicating it to be a shared characteristics of HAB-based prodrugs. It could be argued that liver accumulation may lead to negative effects; however, while no morphological effect was apparent, HABQ did significantly reduce the hepatic level of inflammatory cytokines such as IL1 and IL6 (see Supporting Information, Fig. 5SI). This indicates anti-inflammatory rather than toxic effects, and further confirms the benign character of this formulation.

It is interesting to note a) at 24 h for all HAB derivatives around 70% of the injected dose can still be found (in liver or tumour), while at the same time free quercetin would have been at least half eliminated [23,24]; b) the concentration of HABQ in the tumour was around 70–90 μg per gram of tissue (see Supporting Information, Fig. 4SI), which corresponds to a maximum ~30 nM concentration of quercetin in the tumour for HABQ administered at 10 mg/kg of body weight. Since some quercetin may be released during HABQ circulation, its liberation at the tumoural site would not be instantaneous and it may also diffuse out after liberation, the actual concentration of free quercetin in the tumour

is likely to be significantly lower, i.e. largely insufficient to directly cause cytotoxic effects (see Fig. 1C).

We have then employed a protocol of tail-vein injection every third day for 21 days, in order to verify whether HABQ preferential tumour accumulation was accompanied by therapeutically beneficial effects. The latter was largely ineffective in reducing tumour growth when used at 3 and 6 mg of drug/kg of body weight (growth curve indistinguishable from negative controls such as saline, 11%wt. DMSO, or HAB), with a sound therapeutic effect only observed at 25 mg/kg. HABQ, on the contrary, significantly slowed down tumour growth already at a dosage equivalent to 3 mg quercetin/kg (25 mg/mg of HABQ) with effects similar to those of 25 mg/kg of free quercetin. The effect was even more impressive at a dose equivalent to 6 mg quercetin/kg (50 mg/kg of HABQ). In a direct HABQ/free drug comparison at identical quercetin dosages (see arrows in Fig. 4B), the largest difference is seen at day 27 (6 days after the end of the treatment): at that time point, the tumours treated with 3 and 6 mg quercetin/kg were respectively 2.5 and 5 times smaller with HABQ (Fig. 4C).

In comparison to quercetin, HABQ's much higher antitumoural efficacy can be ascribed to its preferential accumulation, which is likely also responsible of the dose-dependent anti-inflammatory effects of HABQ - but not quercetin – both in the LnCAP xenografted tumour and in the liver (See Supporting Information, Fig. 5SI and 6SI). Besides indicating that HABQ can be regarded as an anti-inflammatory principle in its own right, the lower levels of pro-tumour IL-1b, IL-6 and IL-8 cytokines in the cancer tissue may also contribute to the slower growth of the LnCAP tumour itself. As a partial support to this hypothesis, one has to go back to the actual dose of released quercetin being probably too low to exert directly cytotoxic effects. Although biodistribution experiments were performed at a lower HABQ dose (10 mg/kg), if we assume their % of dose accumulated in the tumour to be comparable to that in therapeutic experiments, one gets an absolutely maximum total (free and bound to HAB) quercetin concentration of ~150 nM. Since – as discussed in the biodistribution paragraph - the actual free drug concentration at the site is a minute faction of this figure, a high direct cytotoxicity seems unlikely (see also Fig. 1C).

4. Conclusions

This study showed the promising therapeutic properties of boronated HA prodrugs in the therapy of prostate cancer. Derivatives based on the HAB structure were indeed shown to be a low-toxicity platform capable of double-responsive release of drugs and preferential accumulation in solid tumours, with liver being the only significant secondary site of accumulation. Considering liver's regenerative capacities, the exposure of this organ to drugs also more toxic than quercetin is of lesser concern than that of e.g. heart or kidneys. Therapeutically, parallel to its enhanced turnout accumulation HABQ also markedly slowed down LnCAP tumour growth, an effect reasonably to ascribe to the localized liberation of quercetin.

Parallel to these encouraging experimental findings, it is worth noting that the knowledge of the in vivo variables affecting the possible mechanisms of accumulation, of release and of pharmacological action is still very incomplete, which makes the results of in vitro experiments sources of plausible indications but not necessarily conclusive answers.

CRediT authorship contribution statement

Vincenzo Quagliariello: Methodology, Investigation, Writing - Original Draft.

Arianna Gennari: Methodology, Investigation.

Som Akshay Jain: Investigation.

Francesco Rosso: Methodology, Supervision.

Rosario Vincenzo Iaffaioli: Supervision.

Alfonso Barbarisi: Conceptualization, Supervision.

Manlio Barbarisi: Conceptualization.

Nicola Tirelli: Conceptualization, Supervision, Writing - Original Draft, Writing - Review & Editing.

Data availability

All of the data reported in this work are available upon request.

Declaration of competing interest

The authors declare that they have no known competing financial interests or personal relationships that could have appeared to influence the work reported in this paper.

Acknowledgments

The University of Campania “Luigi Vanvitelli” is gratefully acknowledged for funding provided to Dr. Quagliariello and Dr. Jain (PhD studentships) and Dr. Rosso (postdoctoral fellowship). Prof. Tirelli and Dr. Gennari gratefully acknowledge Associazione Italiana Ricerca Cancro (AIRC) for financial support through the IG-2020 grant “Hyaluronic acid-based carriers. Targeting mechanisms and application in a combination therapy approach”, project code 24628.

Appendix A. Supplementary data

Supplementary data to this article can be found online at https://doi.org/10.1016/j.msec.2021.112475.

References

[1] J.M.R. de la Rosa, A. Tirella, A. Gennari, I.J. Stratford, N. Tirelli, The CD44-mediated uptake of hyaluronic acid-based carriers in macrophages, Adv. Healthc. Mater. 6 (4) (2017) 1601012.

[2] A. Spadea, J.M.R. de la Rosa, A. Tirella, M.B. Ashford, K.J. Williams, I.J. Stratford, N. Tirelli, M. Mehibel, Evaluating the efficiency of hyaluronic acid for tumor targeting via CD44, Mol. Pharm. 16 (6) (2019) 2481–2493.

[3] J.M.R. de la Rosa, P. Pingrajai, M. Pelliccia, A. Spadea, E. Lallana, A. Gennari, I. J. Stratford, W. Rocchia, A. Tirella, N. Tirelli, Binding and internalization in receptor-targeted carriers: the complex role of CD44 in the uptake of hyaluronic acid-based nanoparticles (siRNA Delivery), Adv. Healthc. Mater. 8 (24) (2019) 1901182.

[4] A. Gennari, M. Pelliccia, R. Donno, I. Kimber, N. Tirelli, Mannosylation allows for synergic (CD44/C-type Lectin) uptake of hyaluronic acid nanoparticles in dendritic cells, but only upon correct ligand presentation, Adv. Healthc. Mater. 5 (8) (2016) 966–976.

[5] S. Ouasti, P.J. Kingham, G. Terenghi, N. Tirelli, The CD44/integrins interplay and the significance of receptor binding and re-presentation in the uptake of RGD-functionalized hyaluronic acid, Biomaterials 33 (4) (2012) 1120–1134.

[6] J.M.R. de la Rosa, A. Tirella, N. Tirelli, Receptor-targeted drug delivery and the (Many) problems we know of: the case of CD44 and hyaluronic acid, Adv. Biosyst. 2 (6) (2018) 1800049.

[7] K.A. Klein, R.E. Reiter, J. Redula, H. Morad, X.L. Zhu, A.R. Brothman, D.J. Lamb, M. Marcelli, A. Belldegrun, O.N. Witte, C.L. Sawyers, Progression of metastatic human prostate cancer to androgen independence in immunodeficient SCID mice, Nat. Med. 3 (4) (1997) 402–408.

[8] N. Mercatelli, V. Coppola, D. Bonci, F. Miele, A. Costantini, M. Guadagnoli, E. Bonanno, G. Muto, G.V. Frajese, R. De Maria, L.G. Spagnoli, M.G. Farace, S. A. Ciafre, The inhibition of the highly expressed Mir-221 and Mir-222 impairs the growth of prostate carcinoma xenografts in mice, PLoS One 3 (12) (2008).

[9] L.Y. Zhuang, J. Kim, R.M. Adam, K.R. Solomon, M.R. Freeman, Cholesterol targeting alters lipid raft composition and cell survival in prostate cancer cells and xenografts, J. Clin. Invest. 115 (4) (2005) 959–968.

[10] T.T. Wu, R.A. Sikes, Q.J. Cui, G.N. Thalmann, C.H. Kao, C.F. Murphy, H. Yang, H. E. Zhau, G. Balian, L.W.K. Chung, Establishing human prostate cancer cell xenografts in bone: induction of osteoblastic reaction by prostate-specific antigen-producing tumors in athymic and SCID/bg mice using LNCaP and lineage-derived metastatic sublines, Int. J. Cancer 77 (6) (1998) 887–894.

[11] J.W. Stevens, P.L. Palechek, T.L. Griebling, R.J. Midura, O.W. Rokhlin, M.B. Cohen, Expression of CD44 isoforms in human prostate tumor cell lines, Prostate 28 (3) (1996) 153–161.

[12] W. Lou, D. Krill, R. Dhir, M.J. Becich, J.T. Dong, H.F. Frierson, W.B. Isaacs, J. T. Isaacs, A.C. Gao, Methylation of the CD44 metastasis suppressor gene in human prostate cancer, Cancer Res. 59 (10) (1999) 2329–2331.

[13] B.L. Lokeshwar, V.B. Lokeshwar, N.L. Block, Expression of CD44 in prostate-cancer cells - association with cell-proliferation and invasive potential, Anticancer Res. 15 (4) (1995) 1191–1198.

[14] D. Zhu, L.Y.W. Bourguignon, The ankyrin-binding domain of CD44s is involved in regulating hyaluronic acid-mediated functions and prostate tumor cell transformation, Cell Motil. Cytoskeleton 39 (3) (1998) 209–222.
[15] E.M. Hurt, B.T. Kawasaki, G.J. Klarmann, S.B. Thomas, W.L. Farrar, CD44(+)CD24 (-) prostate cells are early cancer progenitor/stem cells that provide a model for patients with poor prognosis, Br. J. Cancer 98 (4) (2008) 756–765.
[16] L.L. Zhang, M. Jiao, L. Li, D.P. Wu, K.J. Wu, X. Li, G.D. Zhu, Q. Dang, X.Y. Wang, J. T. Hsieh, D.L. He, Tumorspheres derived from prostate cancer cells possess chemoresistant and cancer stem cell properties, J. Cancer Res. Clin. Oncol. 138 (4) (2012) 675–686.
[17] J. Ni, P.J. Cozzi, J.L. Hao, J. Beretov, L. Chang, W. Duan, S. Shigdar, W.J. Delprado, P.H. Graham, J. Bucci, J.H. Kearsley, Y. Li, CD44 variant 6 is associated with prostate cancer metastasis and chemo-/radioresistance, Prostate 74 (6) (2014) 602–617.
[18] R.J. Williams, J.P.E. Spencer, C. Rice-Evans, Flavonoids: antioxidants or signalling molecules? Free Radic. Biol. Med. 36 (7) (2004) 838–849.
[19] E. Middleton, C. Kandaswami, T.C. Theoharides, The effects of plant flavonoids on mammalian cells: implications for inflammation, heart disease, and cancer, Pharmacol. Rev. 52 (4) (2000) 673–751.
[20] Y. Zhou, J. Zheng, Y. Li, D.P. Xu, S. Li, Y.M. Chen, H.B. Li, Natural polyphenols for prevention and treatment of cancer, Nutrients 8 (8) (2016).
[21] V.C. George, G. Dellaire, H.P.V. Rupasinghe, Plant flavonoids in cancer chemoprevention: role in genome stability, J. Nutr. Biochem. 45 (2017) 1–14.
[22] M. Russo, C. Spagnuolo, I. Tedesco, S. Bilotto, G.L. Russo, The flavonoid quercetin in disease prevention and therapy: facts and fancies, Biochem. Pharmacol. 83 (1) (2012) 6–15.
[23] E.U. Graefe, J. Wittig, S. Mueller, A.K. Riethling, B. Uehleke, B. Drewelow, H. Pforte, G. Jacobasch, H. Derendorf, M. Veit, Pharmacokinetics and bioavailability of quercetin glycosides in humans, J. Clin. Pharmacol. 41 (5) (2001) 492–499.
[24] P.C.H. Hollman, J.M.P. vanTrijp, M. Buysman, M.S. VanderGaag, M.J. B. Mengelers, J.H.M. deVries, M.B. Katan, Relative bioavailability of the antioxidant flavonoid quercetin from various foods in man, FEBS Lett. 418 (1–2) (1997) 152–156.
[25] C. Manach, C. Morand, C. Demigne, O. Texier, F. Regerat, C. Remesy, Bioavailability of rutin and quercetin in rats, FEBS Lett. 409 (1) (1997) 12–16.
[26] N. Orrego-Lagaron, M. Martinez-Huelamo, P. Quifer-Rada, R.M. Lamuela-Ravento, E. Escribano-Ferrer, Absorption and disposition of naringenin and quercetin after simultaneous administration via intestinal perfusion in mice, Food Funct. 7 (9) (2016) 3880–3889.
[27] J.S. Nam, A.R. Sharma, L.T. Nguyen, C. Chakraborty, G. Sharma, S.S. Lee, Application of bioactive quercetin in oncotherapy: from nutrition to nanomedicine, Molecules 21 (1) (2016).
[28] P.C.H. Hollman, J.H.M. Devries, S.D. Vanleeuwen, M.J.B. Mengelers, M.B. Katan, Absorption of dietary quercetin glycosides and quercetin in healthy ileostomy volunteers, Am. J. Clin. Nutr. 62 (6) (1995) 1276–1282.
[29] S. Jeon, C.Y. Yoo, S.N. Park, Improved stability and skin permeability of sodium hyaluronate-chitosan multilayered liposomes by layer-by-layer electrostatic deposition for quercetin delivery 129 (2015) 7–14.
[30] J. Li, J. Zhang, Y.Y. Wang, X. Liang, Z. Wusiman, Y.Z. Yin, Q. Shen, Synergistic inhibition of migration and invasion of breast cancer cells by dual docetaxel/quercetin-loaded nanoparticles via Akt/MMP-9 pathway, Int. J. Pharm. 523 (1) (2017) 300–309.
[31] D. Bennet, S. Kim, A transdermal delivery system to enhance quercetin nanoparticle permeability 24 (2) (2013) 185–209.
[32] X. Pang, Z. Lu, H.L. Du, X.Y. Yang, G.X. Zhai, Hyaluronic acid-quercetin conjugate micelles: synthesis, characterization, in vitro and in vivo evaluation 123 (2014) 778–786.
[33] C.F. Xu, Y. Ding, J. Ni, L.F. Yin, J.P. Zhou, J. Yao, Tumor-targeted docetaxel-loaded hyaluronic acid-quercetin polymeric micelles with p-gp inhibitory property for hepatic cancer therapy, RSC Adv. 6 (33) (2016) 27542–27556.
[34] B.J. Wang, W. Zhang, X.D. Zhou, M.N. Liu, X.Y. Hou, Z.T. Cheng, D.Q. Chen, Development of dual-targeted nano-dandelion based on an oligomeric hyaluronic acid polymer targeting tumor-associated macrophages for combination therapy of non-small cell lung cancer, Drug Deliv. 26 (1) (2019) 1265–1279.
[35] A. Gennari, C. Gujral, E. Hohn, E. Lallana, F. Cellesi, N. Tirelli, Revisiting boronate/diol complexation as a double stimulus-responsive bioconjugation, Bioconjug. Chem. 28 (5) (2017) 1391–1402.
[36] F. Fang, J.-M. Li, Q.-H. Pan, W.-D. Huang, Determination of red wine flavonoids by HPLC and effect of aging, Food Chem. 101 (1) (2007) 428–433.
[37] T. Yoshida, H. Kinoshita, T. Segawa, E. Nakamura, T. Inoue, Y. Shimizu, T. Kamoto, O. Ogawa, Antiandrogen bicalutamide promotes tumor growth in a novel androgen-dependent prostate cancer xenograft model derived from a bicalutamide-treated patient, Cancer Res. 65 (21) (2005) 9611–9616.
[38] A.E.J. de Nooy, G. Masci, V. Crescenzi, Versatile synthesis of polysaccharide hydrogels using the Passerini and Ugi multicomponent condensations, Macromolecules 32 (4) (1999) 1318–1320.
[39] A.P. Bapat, D. Roy, J.G. Ray, D.A. Savin, B.S. Sumerlin, Dynamic-covalent macromolecular stars with boronic ester linkages, J. Am. Chem. Soc. 133 (49) (2011) 19832–19838.
[40] J.J. Cash, T. Kubo, D.J. Dobbins, B.S. Sumerlin, Maximizing the symbiosis of static and dynamic bonds in self-healing boronic ester networks, Polym. Chem. 9 (15) (2018) 2011–2020.
[41] M. Culty, H.A. Nguyen, C.B. Underhill, The hyaluronan receptor (CD44) participates in the uptake and degradation of hyaluronan, J. Cell Biol. 116 (4) (1992) 1055–1062.
[42] H. Harada, M. Takahashi, CD44-dependent intracellular and extracellular catabolism of hyaluronic acid by hyaluronidase-1 and-2, J. Biol. Chem. 282 (8) (2007) 5597–5607.
[43] W. Knudson, G. Chow, C.B. Knudson, CD44-mediated uptake and degradation of hyaluronan, Matrix Biol. 21 (1) (2002) 15–23.
[44] L. Jadin, L.H. Bookbinder, G.I. Frost, A comprehensive model of hyaluronan turnover in the mouse, Matrix Biol. 31 (2) (2012) 81–89.
[45] U.B.G. Laurent, R.K. Reed, Turnover of hyaluronan in the tissues, Adv. Drug Deliv. Rev. 7 (2) (1991) 237–256.
[46] B. McDonald, E.F. McAvoy, F. Lam, V. Gill, C. de la Motte, R.C. Savani, P. Kubes, Interaction of CD44 and hyaluronan is the dominant mechanism for neutrophil sequestration in inflamed liver sinusoids, J. Exp. Med. 205 (4) (2008) 915–927.
[47] B. McDonald, P. Kubes, Interactions between CD44 and hyaluronan in leukocyte trafficking, Front. Immunol. 6 (2015) 6.
[48] G.A. Potter, L.H. Patterson, E. Wanogho, P.J. Perry, P.C. Butler, T. Ijaz, K. C. Ruparelia, J.H. Lamb, P.B. Farmer, L.A. Stanley, M.D. Burke, The cancer preventative agent resveratrol is converted to the anticancer agent piceatannol by the cytochrome P450 enzyme CYPIBI, Br. J. Cancer 86 (5) (2002) 774–778.